



Shaking Table Model Test to Determine Dynamic Response Characteristics and Failure Modes of Steep Bedding Rock Slope

Jinyu Dong¹ · Chuang Wang¹ · Zhiquan Huang² · Jihong Yang¹ · Lei Xue^{3,4}

Received: 6 July 2021 / Accepted: 15 February 2022 / Published online: 19 March 2022
© The Author(s), under exclusive licence to Springer-Verlag GmbH Austria, part of Springer Nature 2022

Abstract

A model of a steep bedding rock slope with a slope angle of 50° and rock dip angle of 55° was designed and fabricated, and a large-scale shaking table test was carried out to investigate the acceleration, displacement, acoustic emission, and failure mode under earthquake action. In the vertical direction of the slope, the acceleration amplification factor significantly increased as the elevation increased. In the horizontal slope direction, the acceleration amplification factor decreased with the distance from the slope surface. Under the action of different input wave types, the acceleration response of the slope was markedly different. The acceleration amplification factor exhibited the change law of first increasing and then decreasing with the increase in the input wave frequency, and became maximum when the frequency was 25 Hz. With the increase in the input wave amplitude, the acceleration amplification factor of the slope exhibited the trend of first increasing and then decreasing. The slope displacement and the acoustic emission parameters increased nonlinearly with the increase in the input wave amplitude, and the process can be divided into two stages: the slow increase period and the sharp increase period. Under seismic wave action, the deformation and failure evolution process of the slope included four stages: (1) the rock layer at the top of slope undergoes tension fracture; (2) the tensile cracks extend downward along the layer to form a locked segment at the toe of the slope; (3) the locked segment shear fractures through the sliding surface; (4) the slope suddenly becomes unstable and slides. The failure mode of the slope model was tension-shear sliding failure.

Highlights

- Acceleration response law of steep bedding rock slope under earthquake action was studied.
- Acoustic emission characteristics of steep bedding rock slope under earthquake action was analyzed.
- Deformation and failure modes of steep bedding rock slope under earthquake action were analyzed.
- Locked segment had play a key role on steep bedding rock slope stability under earthquake action.

Keywords Steep bedding rock slope · Large-scale shaking table test · Dynamic response characteristics · Acoustic emission technology · Failure mode

✉ Chuang Wang
wangchuang@ncwu.edu.cn

¹ Research Institute of Geotechnical Engineering and Hydraulic Structure, North China University of Water Resources and Electric Power, Zhengzhou 450046, China

² Luoyang Institute of Science and Technology, Luoyang 471023, China

³ Key Laboratory of Shale Gas and Geoengineering, Institute of Geology and Geophysics, Chinese Academy of Sciences, Beijing 100029, China

⁴ Innovation Academy for Earth Science, Chinese Academy of Sciences, Beijing 100029, China

1 Introduction

With the implementation of China's western development strategy and the continuous development of the national economy, the number of large-scale and super large-scale hydropower projects and traffic municipal engineering projects in mountainous areas has gradually increased. In the Sichuan-Chongqing area in particular, there is a large number of natural bedding high-steep slopes and engineered high-cut slopes along the project line, owing to the complex geological and topographical conditions of this mountainous area and frequent earthquake disasters. A steep bedding slope with a dip angle greater than the slope angle is more stable under natural conditions, but can easily become unstable and form a high-speed long-distance landslide under earthquake action (Huang et al. 2012; Cui et al. 2018; Zhao et al. 2020). For example, the Tangjiashan landslide is a typical example of the seismic dynamic instability of a steep bedding slope (Hu et al. 2009; Chen et al. 2011; Liu et al. 2012; Xu et al. 2013). The survey data show that the topographical slope of Tangjiashan was 40° before the earthquake, had a medium steep slope structure, and was stable. A high-speed landslide formed under the Wenchuan earthquake. The sliding time of the entire landslide was approximately 0.5 min and the relative sliding displacement was 900 m. On one occasion, a barrier lake formed and posed a major threat to the safety of 300,000 people located downstream in Mianyang City (Chigira et al. 2010; Hu et al. 2011; Qi et al. 2015; Shi et al. 2015; Kidyeva et al. 2017). Therefore, the investigation of the dynamic response and instability mechanism of a steep bedding slope in high-intensity seismic areas has great theoretical and practical significance.

The shaking table model test is one of the most effective methods for studying the strong earthquake response and failure mode of slopes, and has been widely used in the dynamic response analysis of different slope structures (Hsieh et al. 2011; Janusz et al. 2011; Liu et al. 2014; Che et al. 2016; Chen et al. 2016). Dong et al. (2011, 2013) conducted a large-scale shaking table test on a bedding rock slope, investigated the failure mode of the bedding slope under dynamic action, and analyzed the influence of the input wave's waveform, frequency, and amplitude on the dynamic slope response. Wang and Lin (2011) and Nakajima et al. (2016) investigated the progressive failure of slopes through shaking table tests. Xu et al. (2010), Huang et al. (2013), and Li et al. (2019) investigated the instability and failure process of slopes with different structure types under strong earthquakes by carrying out shaking table model tests on rock mass slopes with anti-dip and bedding structures. Wartman et al. (2005) investigated the permanent displacement of an earthquake-induced landslide by carrying out shaking

table tests. Srilatha et al. (2013) investigated the influence of the seismic wave frequency on the dynamic response of a reinforced slope by carrying out a shaking table model test. Yang et al. (2017) compared the dynamic responses of a bedding-structure slope and homogeneous-structure slope obtained using a large-scale shaking table model test. Fan et al. (2016) conducted a large-scale shaking table test on a bedding rock slope with a soft interlayer, and investigated the influence of the input seismic wave characteristics and muddy interlayer saturation condition on the dynamic response of the bedding rock slope.

This study used the large-scale shaking table test method, and a steep bedding rock slope model with a slope angle of 50° and a rock dip angle of 55° was designed and manufactured. A large-scale shaking table test was carried out to investigate the dynamic response of the acceleration, displacement, acoustic emission, and deformation failure mode of the bedding rock slope under a seismic wave. The results can provide a basis for the dynamic stability evaluation and reinforcement design of this slope type.

2 Design of Shaking Table Model Test

2.1 Similarity Ratio Design and Similar Materials

Considering the difficulty entailed in the dynamic testing of a rock slope under field conditions, the scale model test for rock slopes was adopted with consideration to practicality and cost efficiency. To simulate the actual project, the geometric dimensions of the test model and the main physical and mechanical properties considered in the model test should be as similar as possible to those of the prototype. In the model test, the ratio of the physical quantity corresponding to the prototype and physical model was defined as the similarity coefficient C_i (i is the corresponding parameter). Based on the Buckingham theorem (Buckingham 1914) and

Table 1 Main similarity constants in model test

Physical quantities	Similarity relation	Similarity coefficient
Density (ρ)	C_ρ	1
Length (L)	C_L	16
Time (t)	C_t	4
Young's modulus (E)	$C_E = C_\rho C_L^2 C_t^{-2}$	16
Poisson's ratio (μ)	C_μ	1
Internal friction angle (φ)	C_φ	1
Cohesion (c)	$C_c = C_E$	16
Acceleration (a)	$C_a = C_E C_\rho^{-1} C_L^{-1}$	1
Frequency (f)	$C_f = C_t^{-1}$	0.25
Stress (σ)	$C_\sigma = C_E C_\rho$	16

the dynamic similarity conditions, the similarity relationship of various physical quantities was determined by considering the geometric, physical, and motion conditions. In the shaking table model test, the 10 parameters listed in Table 1, including the density ρ , length L , and time t , were selected as the control parameters.

Slope model tests are mostly indoor scale tests. Therefore, the selection of similar materials must satisfy the characteristics of low elastic modulus and high capacity weight. Moreover, satisfactory test accuracy and good processing performance are required. Many domestic and overseas studies have investigated similar materials for tests using engineering geomechanical models (Luo and Ge 2008; Meguid et al. 2008). In this experiment, similar slope materials were selected from the research results of Dong et al. (2012), and consisted of barite powder, iron concentrate powder, and quartz sand as the main material, and gypsum as the auxiliary material. A rosin alcohol solution was made by mixing adhesive materials, and the mass ratio of iron powder, barite powder, quartz sand, gypsum, rosin, and alcohol was 7.4:66.3:31.6:7.1:1:5.7. The physical and mechanical parameters of the similar materials were determined by laboratory tests, as follows: density of 2.50 g/cm³; compressive strength of 0.853 MPa; tensile strength of 0.099 MPa; elastic modulus of 124.46 MPa; Poisson's ratio of 0.12; internal friction angle of 34.8°; cohesion of 0.294 MPa.

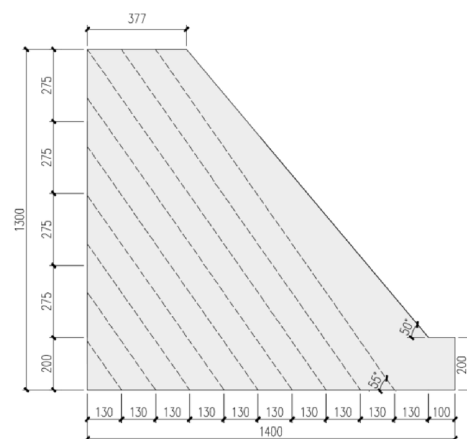
2.2 Design and Fabrication of Steep Bedding Slope Model

Generally, the rigid model box is used in the shaking table test of the rock slope mode. A rigid model box with the size 150 cm × 85 cm × 150 cm (length × width × height) was

designed for the test. Two transparent organic glass plates with a thickness of 10 mm were installed as the front and rear sidewalls to observe the deformation of the slope model. Due to the wear resistance of organic glasses, thereby rendering these two walls sliding boundaries, so the side of the model does not require additional treatment (Ning et al. 2019; Yang et al. 2020; Dong et al. 2021; Panah and Eftekhari 2021). To minimize the boundary effect, a polystyrene foam board with the thickness of 10 cm was placed on the broadside of the rigid box, and a 10 cm thick buffer layer made of the same model materials as the slope was installed at the bottom boundary. Although the boundary effect of the rigid container was not completely eliminated in this shaking table test, reasonably correct test data were still obtained under this condition (Whitman and Lambe 1986; Wartman et al. 1998 and 2005; Yang et al. 2017).

The experimental design of the steep bedding rock slope model had the following dimensions: height of 130 cm, width of 83 cm, and length of 140 cm; the slope angle was 50°; the rock layer thickness was 13 cm; the rock layer dip angle was 55°. The model slope was built in the model box and compacted layer by layer from the bottom to the top. First, the required materials for each layer were identified, mixed and shoveled into the model box. Second, a made rammer was used to compact the wet-stirred material. Third, a thin layer of mica powder was evenly spread on the bedding plane after each layer was compacted. The accelerometers embedded in the slope interior were buried during the construction of the slope, and the accelerometers embedded on the slope surface were installed after the slope was completed. These steps were repeated until the slope model reached the designed height. The sizes of the model slope and the completed model slope are shown in Fig. 1.

Fig. 1 Steep bedding rock slope model: **a** configuration of scaled slope model (unit: mm); **b** photo of finished model slope



(a)



(b)



Fig. 2 Shaking table equipment

2.3 Testing Device

The shaking table had a size of 3 m × 3 m and capacity of 10,000 kg; the loading frequencies ranged from 0.5 to 50 Hz. The accelerations under full loading in the X, Y, and Z directions ranged from -1.0 to 1.0 g, as shown in Fig. 2. The displacements under full loading in the X and Z directions ranged from ± 150 mm to ± 150 mm, and the range of the velocities in the X and Z directions ranged from -700 to 700 mm/s and -700 to 700 mm/s, respectively.

2.4 Measuring Instrument

The slope acceleration response and its distribution law are the main data needed to evaluate the slope’s seismic dynamic response characteristics. The acceleration sensor used in the test is the IEPE unidirectional acceleration sensor, which was matched with the DH8032 dynamic signal test and analysis system. The sensitivity was 100 mV/g and the frequency response was 0.5–100.0 Hz. To quantitatively describe the dynamic changes of the slope model with limited data acquisition channels, acceleration sensors were arranged as much as possible, and a row of acceleration sensors was arranged along the slope surface and at different elevations within the slope. Moreover, a unidirectional acceleration sensor A0 was arranged onto the table to control the acceleration input during the test. The sensor arrangement is shown in Fig. 3.

The displacement test used a 3D laser scanner. In the experiment, the 3D coordinate information of the slope table was obtained by the 3D laser scanner before and after the seismic wave input, and the overall deformation characteristics of the slope surface before and after the test were

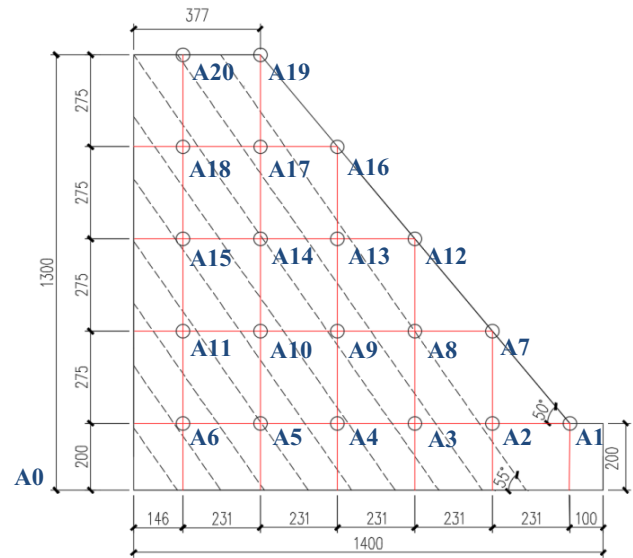


Fig. 3 Layout of acceleration transducer (unit: mm)

obtained by comparing the data before and after the test. The FARO 3D laser scanner Focus3D X330 was used in this experiment. The accuracy of the Faro 3D laser scanner is 2 mm. The setup of the 3D laser scanner and the placement of the target ball are shown in Fig. 4.

In the test, the acoustic emission signals generated by the energy release of the slope model under seismic loading were monitored by the acoustic emission probes arranged on the slope surface. The acoustic emission monitoring system used in this test was the PCI-II acoustic emission system

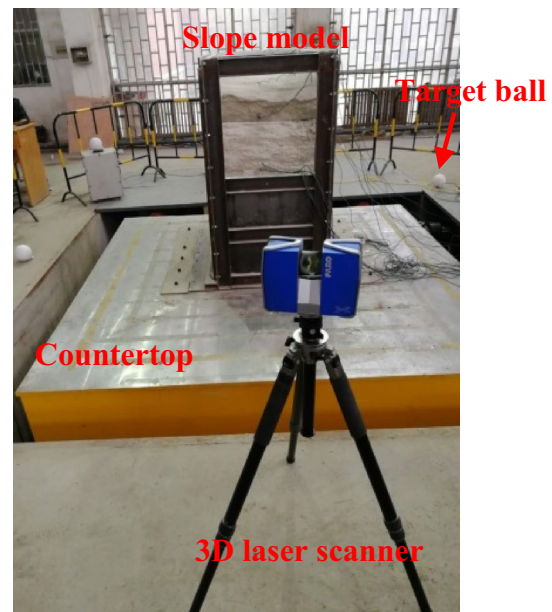


Fig. 4 Displacement measuring equipment



Fig. 5 Layout of acoustic emission probe

produced by an American acoustic physics company, and mainly consists of the acoustic emission probe, signal amplifier, acoustic emission card, and acoustic emission acquisition software. The layout of the acoustic emission probe in the test is shown in Fig. 5.

2.5 Input motions

The purpose of this test was to investigate the influence of the seismic wave type, frequency, and amplitude on the dynamic response characteristics of the steep bedding rock slope. During the test, the Wolong (WL) seismic wave, EI Centro wave, and a sine wave with a low amplitude of 0.1–0.2 g were first applied to the model to investigate the dynamic response of the slope without large deformation and failure. According to the similarity criterion, the WL wave and EI wave were compressed according to the time similarity coefficient ($C_t=4$) (Fig. 6); the input direction was X unidirectional; the frequency of the input sine wave was 5 Hz, 10 Hz, 15 Hz, 20 Hz, 25 Hz, 30 Hz, 35 Hz, and 40 Hz; the excitation direction was also the X direction, and the duration was 20 s. Then, the amplitude of the WL wave and 10 Hz sine wave was gradually increased to 0.3 g, 0.4 g, ..., 0.6 g, and the deformation and failure evolution mode of the slope was investigated under the action of a seismic wave

Fig. 6 Acceleration history of natural seismic wave: a) time history of WL wave; b) fourier spectrum of WL wave; c) time history of EI wave; d) fourier spectrum of EI wave

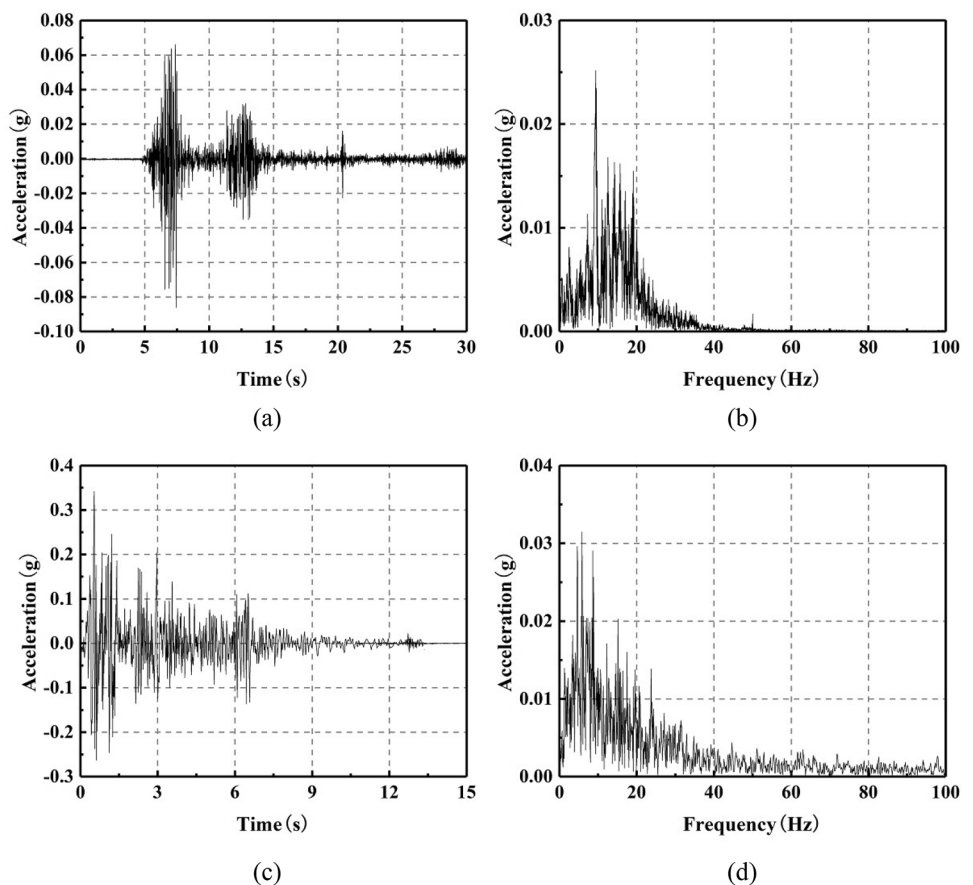


Table 2 Test loading sequence

Number	Waves	Amplitude (g)	Frequency (Hz)
1	WL wave	0.1	–
2	EI wave	0.1	–
3–10	Sine wave	0.1	5, 10, 15, 20, 25, 30, 35, 40
11	WL wave	0.2	–
12	EI wave	0.2	–
13–20	Sine wave	0.2	5, 10, 15, 20, 25, 30, 35, 40
21	WL wave	0.3	–
22	Sine wave	0.3	10
23	WL wave	0.4	–
24	Sine wave	0.4	10
25	WL wave	0.5	–
26	Sine wave	0.5	10
27	WL wave	0.6	–
28	Sine wave	0.6	10

with gradually increasing amplitude. The input scheme is presented in Table 2.

3 Analysis of Test Results

3.1 Acceleration Response Characteristics of Slope Model

3.1.1 Distribution Law of Slope's Acceleration Response

The inertial force generated by the seismic acceleration is the main reason for the dynamic deformation and instability of the slope under earthquake action, and the acceleration change and distribution law in the slope are the basic information required to evaluate the slope's seismic dynamic response. According to previous results (Latha and Garaga 2010; Gischig et al. 2015; Song et al. 2018), the ratio of the peak acceleration of the dynamic response at each measuring point to the peak acceleration measured on the table surface is defined as the acceleration amplification factor.

To obtain the overall distribution law of the slope acceleration response, the contour maps of the acceleration amplification factor under a 0.1 g and 0.2 g WL wave, EI wave, and sine wave excitation were drawn according to the test data, as shown in Fig. 7. The test results reveal that, in the vertical direction, the acceleration amplification factor markedly increased as the slope height increased. In particular, the acceleration amplification coefficient was maximum at the shoulder of the slope. In the horizontal direction, the acceleration amplification factor exhibited an obvious amplification effect in a certain range of depth from the slope surface. Moreover, the amplitude of the input wave also affected the acceleration amplification factor. With an input wave amplitude

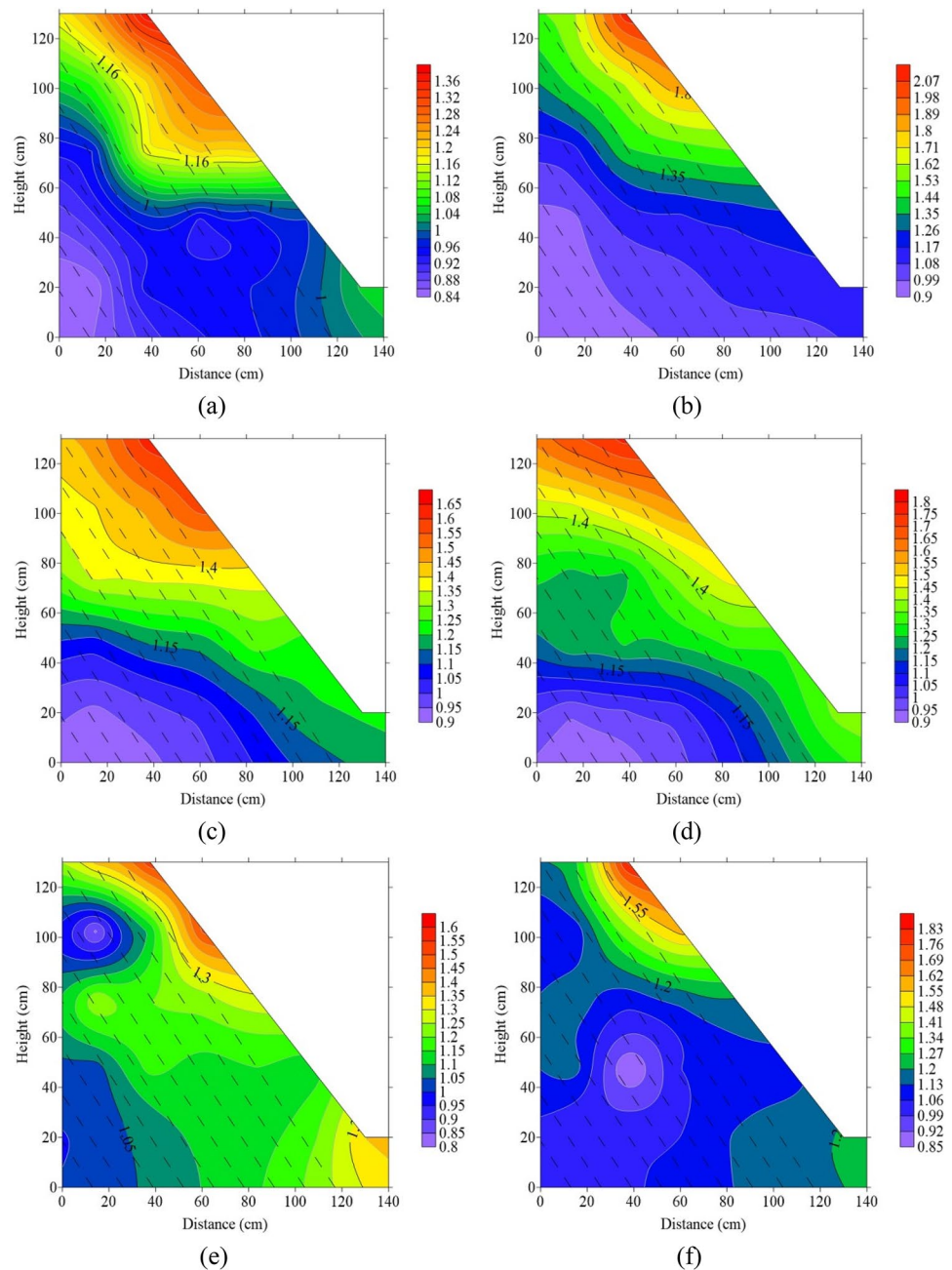
of 0.2 g, the acceleration amplification factor of slope was greater than that with an input wave amplitude of 0.1 g.

Figure 8 shows the amplification law of the vertical and horizontal acceleration response of the slope surface and slope body under a sine wave with a frequency of 10 Hz, EI wave, and WL wave with an amplitude of 0.2 g. As can be seen from Fig. 8a, the acceleration amplification factor increased nonlinearly with the elevation increase. When the slope height was less than 0.75 m, the acceleration amplification factor increased slowly. When the slope height was greater than 0.75 m, the acceleration amplification factor significantly increased as the slope height increased. The maximum amplification factor of the 0.2 g sine wave with a frequency of 10 Hz was 1.85, the amplification factor of the 0.2 g EI wave was 1.77, and the amplification factor of the 0.2 g WL wave was 2.13. In the vertical direction inside the slope (measuring points A5, A10, A14, A17, and A19), as the elevation increased, the acceleration amplification factor gradually increased and reached the maximum value at the top of the slope, which demonstrates the elevation amplification effect. As shown in Fig. 8b, the acceleration amplification factor increased from 0.99 to 1.77 under the EI wave excitation, and from 1.01 to 2.13 under the WL wave excitation. As can be seen, the increase in the acceleration amplification factor with the elevation was more significant. Figure 8c shows that, in the horizontal direction with the same slope elevation (measuring points A15, A14, A13, and A12), the acceleration amplification factor of the slope increased as the distance from the slope surface decreased. Additionally, the acceleration amplification factor inside the slope was smaller than that of the slope surface, the acceleration magnification factor of measuring point A15 on the slope of EI wave excitation was 1.23, the acceleration amplification factor of the slope surface measuring point A12 was 1.46, the acceleration amplification factor of measuring point A15 on the slope under WL wave excitation was 1.13, and the acceleration amplification factor of the slope meter measuring point A12 was 1.53; that is, the acceleration response in the horizontal direction exhibited a trending effect.

3.1.2 Influence of Waveform on Slope Acceleration Response

We considered the sine wave (frequency of 10 Hz), EI wave, and WL wave with the input wave amplitude of 0.2 g as an example, and compared the variation law of the acceleration amplification factor with elevation at the slope surface (Fig. 8a). The comparison revealed that there are obvious differences in the acceleration response of the slope under the action of different input wave types. Generally, the increase factor of the natural seismic wave on the slope surface was significantly higher than that of the sine wave,

Fig. 7 Contour map of acceleration amplification coefficient: **a** 0.1 g WL wave; **b** 0.2 g WL wave; **c** 0.1 g EI wave; **d** 0.2 g EI wave; **e** 0.1 g sine wave; **f** 0.2 g sine wave



mainly owing to the uneven distribution of the actual seismic wave energy. Fan et al. (2016) pointed out that the uneven distribution of seismic energy has a significant impact on the dynamic response of the slope. Moreover, as revealed by the test results, the EI wave and WL wave have different spectral characteristics in the slope acceleration response.

3.1.3 Influence of Frequency on Slope Acceleration Response

To analyze the influence of the input wave frequency on the slope acceleration response, a sine wave excitation

with an amplitude of 0.1 g and 0.2 g and different frequencies was used in the test. The relationship curves between the acceleration amplification factor on the slope surface and the input wave frequency are shown in Fig. 9. As revealed by the test results, the frequency of the input wave significantly affected the acceleration response of the slope. The acceleration amplification factor first increased and then decreased with the increase in the input wave frequency, and reached its maximum value when the frequency of the sine wave was 25 Hz. Moreover, with the increase in the relative height of the measuring point, the frequency exerted increasingly more

Fig. 8 Acceleration dynamic response of slope model: **a** acceleration amplification factor on slope surface; **b** acceleration amplification factor inside slope in vertical direction; **c** acceleration amplification factor inside slope in horizontal direction

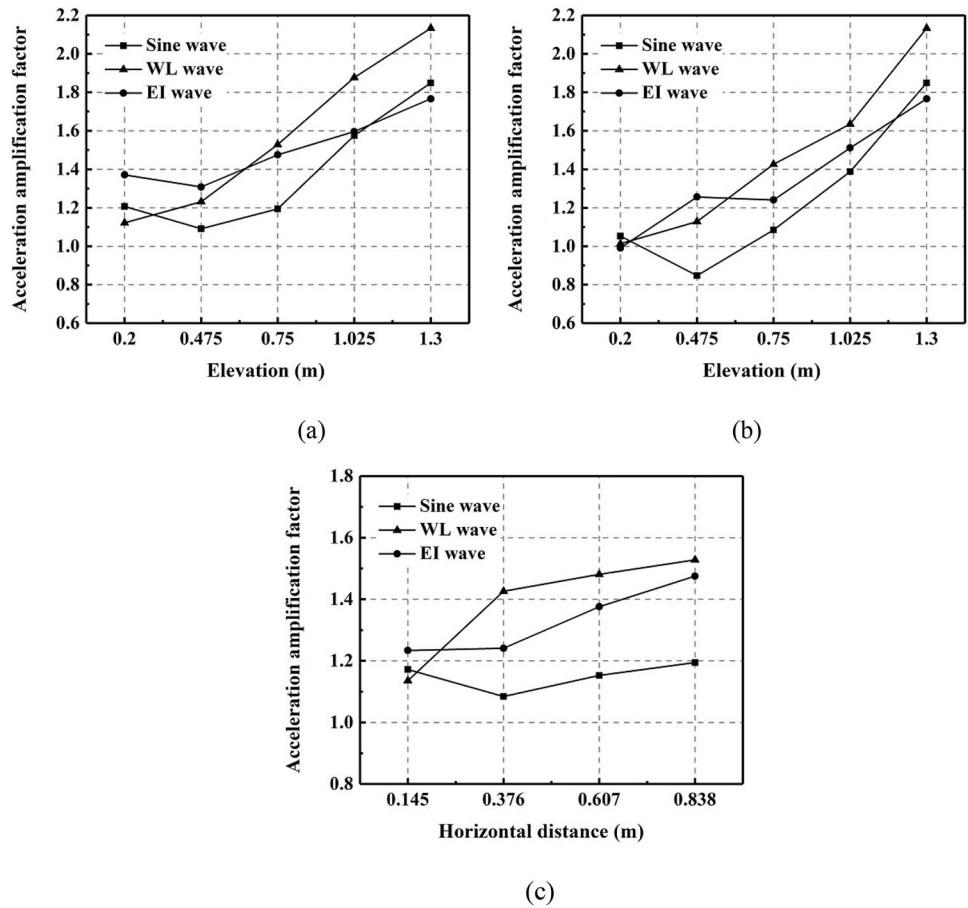
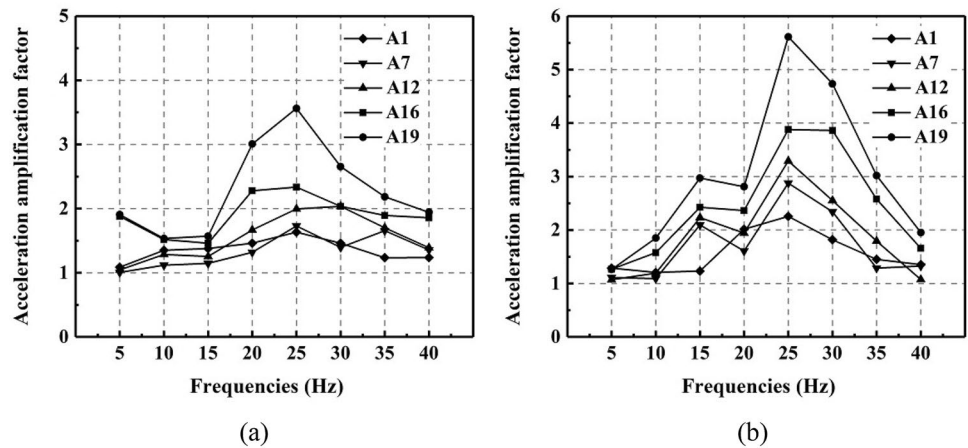


Fig. 9 Acceleration amplification factor of slope surface under sine wave input with different frequency: **a** amplitude of 0.1 g; **b** amplitude of 0.2 g



influence on the amplification factor of acceleration. The acceleration amplification factor of the different measuring points of the slope surface under the action of a 0.2 g sine wave with a frequency of 25 Hz was considered as an example. The acceleration amplification factor values for

measuring point A1 (elevation 0.2 m), measuring point A7 (elevation 0.457 m), measuring point A12 (elevation 0.75 m), measuring point A15 (elevation 1.025 m), and measuring point A19 (elevation 1.3 m) were 2.26, 2.88, 3.29, 3.88, and 5.61, respectively.

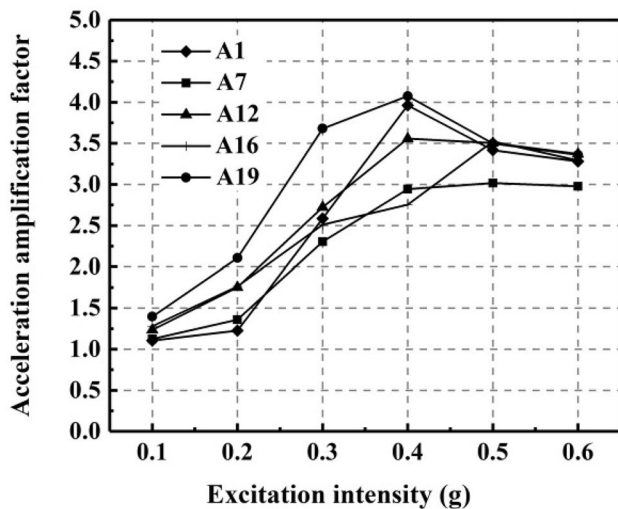


Fig. 10 Effect of input wave amplitude on slope acceleration amplification factor

3.1.4 Influence of Amplitude on Slope Acceleration Response

The input scheme of different amplitudes was adopted for the sine wave. By considering the variation law of the acceleration amplification factor of the slope surface under the 10 Hz sine wave excitation as an example, the influence of the input wave amplitude on the slope acceleration response was analyzed. Figure 10 shows the relationship curve for the acceleration amplification factor on the slope surface and the input wave amplitude. The test results reveal that the acceleration amplification factor first increased and then decreased as the amplitude increased. When the input amplitude was less than 0.4 g, the acceleration amplification factor of the slope model increased with the input amplitude value. However, when the input seismic amplitude value was larger than 0.4 g, the acceleration amplification factor of the slope model decreased with the increase in the input seismic amplitude value.

This phenomenon is related to the nonlinear and damping properties of slope materials and the frequency characteristics of the earthquake wave. When the seismic wave amplitude was small, the slope was in the elastic deformation stage, which made the acceleration amplification factor increase with the input wave amplitude. When the input seismic wave amplitude reached 0.4 g, the shear strain of the slope increased and the shear modulus decreased, which led to the decrease of the slope's natural frequency. Additionally, the hysteretic curve became wider, the damping ratio increased, and the slope model dissipated more energy. At the same time, the

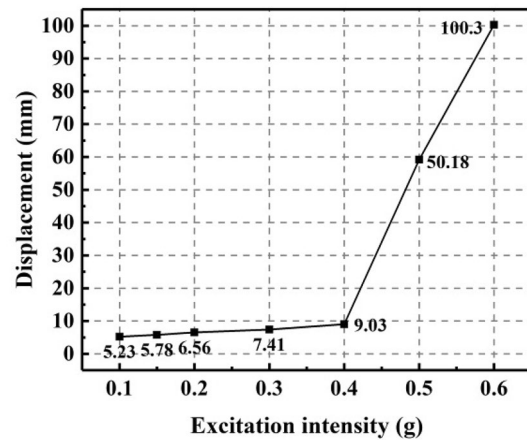


Fig. 11 Relationship between monitoring point displacement and input amplitude value

material also exhibited nonlinear characteristics. With the increase in the input amplitude, the filtering effect of the material was enhanced. Notably, these factors weakened the dynamic response of the material, which leads to the decrease of the acceleration amplification factor as the input wave amplitude increases.

3.2 Slope Displacement Response Characteristics

During the test, displacement monitoring was carried out at slope measuring point A16, as shown in Fig. 3. Figure 11 shows the relationship curve for the displacement of the monitoring point and the amplitude of the input wave acceleration. The test results reveal that the slope surface displacement of the steep bedding rock slope also exhibited the change rule of nonlinear increase with the increase in the input wave amplitude. The slope surface displacement can be divided into two stages: the slow increase period and the sharp increase period. When the input amplitude was less than 0.4 g, the displacement at the slope surface measuring point A16 only increased from 5.23 to 9.03 mm, and the increase was slow. However, when the input wave amplitude reached 0.4 g, the displacement value at measuring point A16 increased from 9.03 to 100.3 mm, and the increase in the displacement value was extremely significant.

3.3 Response Characteristics of Slope Acoustic Emission Parameters

With the increase in the input wave amplitude, the corresponding acoustic emission parameters continuously changed, and all of them exhibited the change law of nonlinear increase, as shown in Fig. 12. When the input wave amplitude was less than 0.2 g, the acoustic emission energy, acoustic emission amplitude, and acoustic

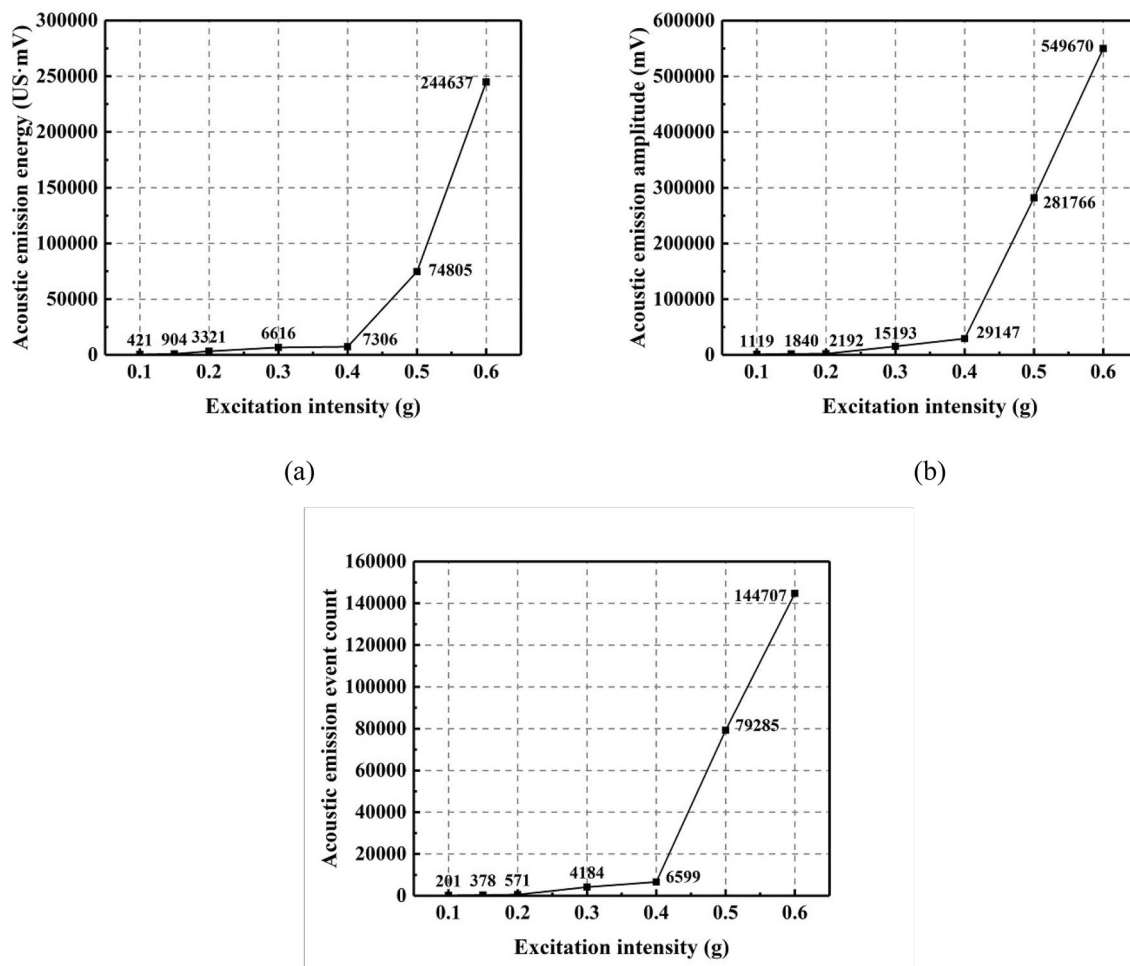


Fig. 12 Variation law of acoustic emission characteristic parameters of model slope under seismic wave excitation: **a** acoustic emission energy; **b** acoustic emission amplitude; **c** acoustic emission event count

emission count changed very little, which indicates that the slope was in the stage of elastic compaction deformation—that is, the process of energy storage. When the input wave amplitude was between 0.3 and 0.4 g, there were many macroscopic fine cracks inside the slope, and acoustic emission activity occurred frequently and continuously, which led to a certain increase in the acoustic emission energy, acoustic emission amplitude, and acoustic emission count, but without significant fluctuation. However, when the input amplitude reached 0.4 g, cracks appeared on the slope surface and the sudden shearing of the locked segment made the acoustic emission activity more intense and led to a sharp increase in the acoustic emission energy, acoustic emission amplitude, and acoustic emission count.

Therefore, according to the test results, the acoustic emission characteristics of the steep bedding slope can be divided into two stages: the slow increase period and

the sharp increase period. In the slow increase period, tiny cracks appeared inside the slope and gradually accumulated. When the sharp increase stage was reached, the locked segment that formed inside the slope sheared off, and the slope underwent large deformation and eventually failure. As can be seen, the acoustic emission characteristics can be used as predictive and early warning indicators for slope deformation and failure.

3.4 Failure Mode Analysis of Slope

During the test, the deformation of the slope model was carefully observed and photographed after each input wave excitation was applied, and the entire test process was also photographed to analyze the failure characteristics and failure mode of the slope model. Figure 13 shows the deformation and failure of the slope model during the test. A small tensile crack was generated at the shoulder of the slope top

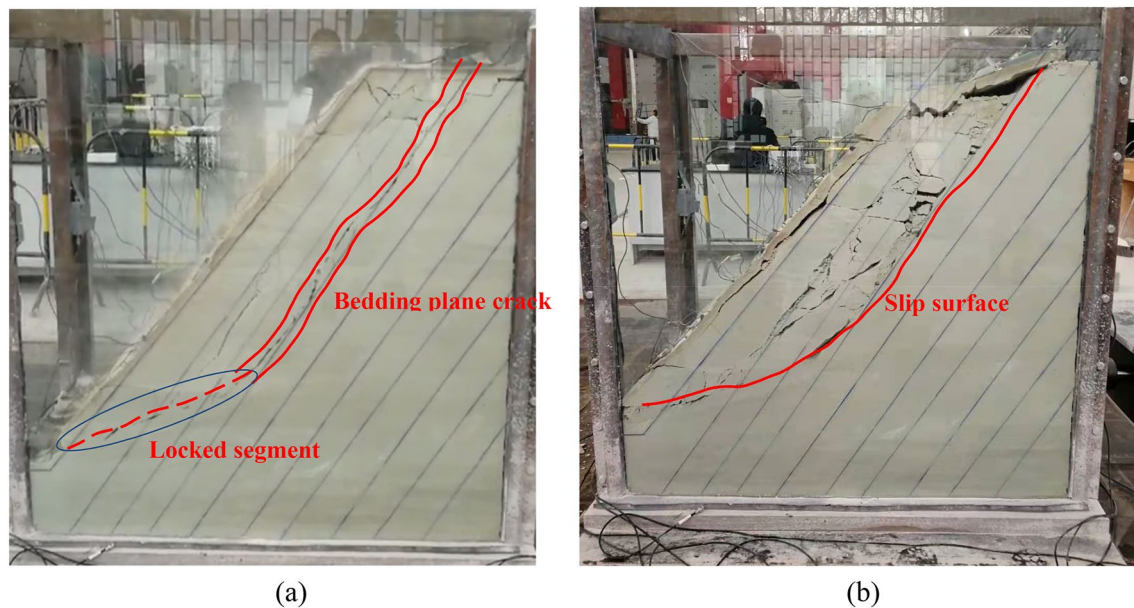


Fig. 13 Photographs of dynamic failure of steep bedding slope: **a** locked segment is sheared; **b** sliding failure of slope occurs

during the test wherein a sine wave with an amplitude of 0.3 g was used as input. When the sine wave with an amplitude of 0.4 g was used as input, the tensile crack extended downward along the layer surface and formed a locked segment at the toe of the slope. The stability of the slope was mainly supported by this locked segment (Fig. 13a). Then, when the sine wave with an amplitude of 0.5 g was used as input, the locked segment at the toe of the slope sheared and penetrated into the layer cracks to form a slip surface, which produced the sliding failure of the slope. Finally, under the action of the sine wave with an amplitude of 0.6 g, the top of the slope was pulled and cracked layer by layer, and the slope was further damaged by the sliding (Fig. 13b).

According to the deformation and failure process observed in the large-scale shaking table test on the steep bedding rock slope model, the evolution of deformation and the failure mode of the steep bedding rock slope under seismic dynamic action can be divided into four stages:

1. Stage of tensile crack formation at top of slope

The dip angle of the rock layer in the steep bedding rock slope was greater than the slope angle and the stability was better under natural conditions. However, the rock layer in the slope was the weakest link in the slope. Under seismic wave action and the elevation effect of seismic acceleration, the rock mass close to the slope shoulder was the part with the largest stress change, which resulted in the emergence of the first tensile crack along the rock layer, as shown in Fig. 14a.

2. Tensile crack extends downward and locked segment forms at slope toe.

Because the rock layer was the weakest link in the slope, under the action of the horizontal seismic force, the cracks and rock layer had the characteristics of tension, and tension cracks gradually extended downward along the rock layer in the slope. After the tension crack had formed at the back edge, a locked segment of the slope formed at the front edge of the slope toe, and the stability of the slope was mainly supported by this locked segment, as shown in Fig. 14b.

3. Stage of locked segment shearing and rupture, and sliding surface transfixion.

Under the continued action of earthquake loading, stress concentration occurred at the locked segment that formed at the lower part of the slope. Under the combined action of the strong seismic force and upper sliding force, the cumulative amount of rock mass stress in the locked segment at the lower part of the slope exceeded the rock mass. With the sudden shear failure of the locked segment, the shear section of the locked segment and the tensile cracks of the slope rock surface combined to form a through sliding surface, as shown in Fig. 14c.

4. Stage of slope sliding.

With the continuation of seismic loading, owing to the shear of the locked segment, the upper and middle sliding mass lost its support and slid along the through sliding surface to the free-face direction. The entire landslide was destroyed by sliding. At the same time, the inner rock layer at the top of the slope broke layer by layer under the seismic wave action, owing to the loss of restraint, and the slope was further damaged as

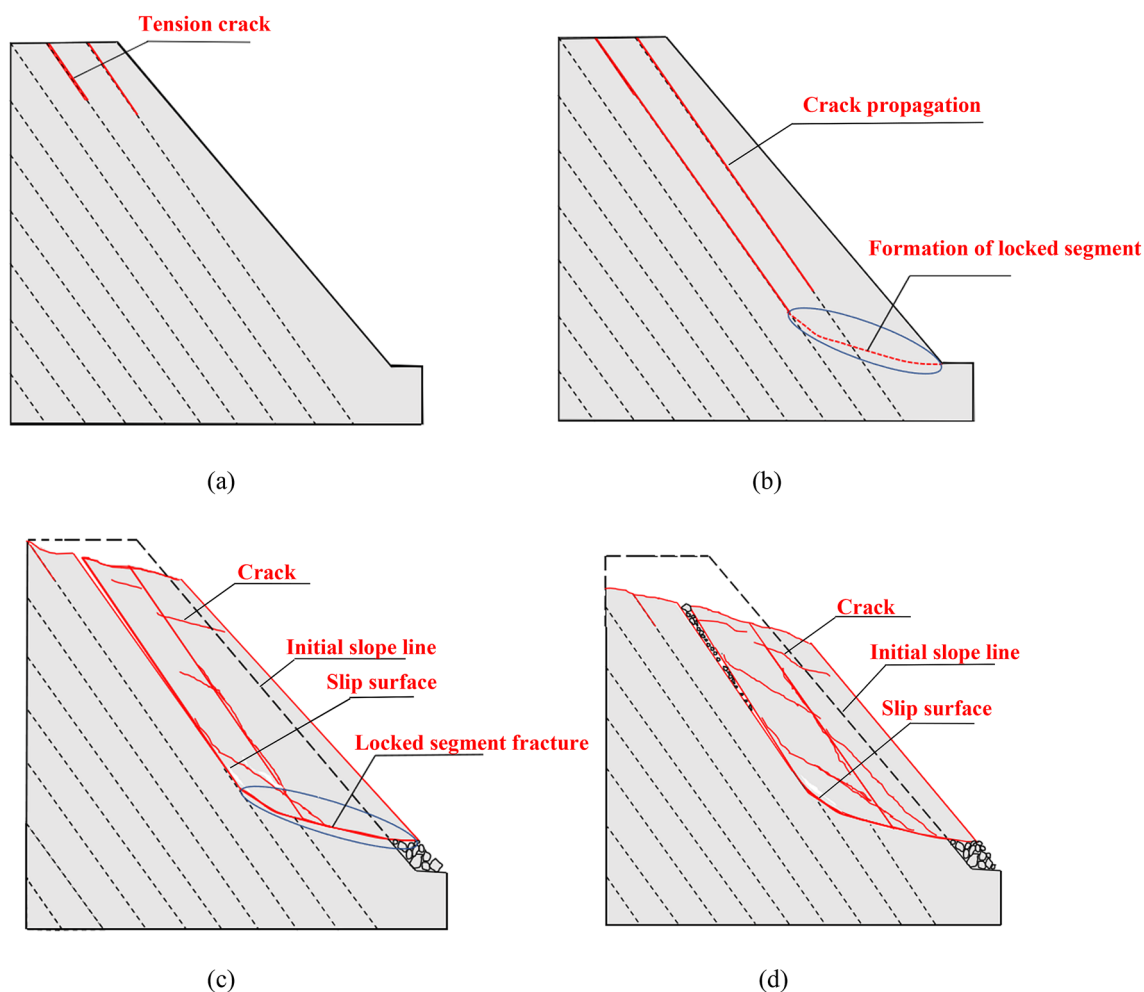


Fig. 14 Failure diagram of steep bedding slope under seismic dynamic action: **a** tensile cracks on top of slope; **b** tensile crack extends downward and forms a locked segment; **c** locked segment suddenly shears and sliding surface is connected; **d** sliding failure of slope occurs

shown in Fig. 14d. Therefore, the failure mode of the steep bedding rock slope under seismic dynamic action was tension-shear sliding failure.

4 Conclusions

The following conclusions were drawn from this study:

1. In the vertical direction of the slope and inside the slope, the acceleration amplification factor increased nonlinearly with the increase in the slope height, and the acceleration response exhibited an elevation amplification effect. In the horizontal slope direction, the acceleration amplification factor increased as the distance from the slope surface decreased, and the acceleration response exhibited a surface effect. Additionally, the contour map of the acceleration amplification factor in the slope was obtained according to the results of the shaking table model test.
2. Under the action of different input wave types, there were obvious differences in the slope's acceleration responses. The acceleration response of the model slope to the natural seismic wave was stronger compared with the response to the sine wave. The slope acceleration amplification factor first increased and then decreased with the increase in the input frequency, and reached its maximum value when the frequency was 25 Hz. As the amplitude of the input wave increased, the acceleration amplification factor also exhibited the change law of first increasing and then decreasing.
3. Under the action of horizontal dynamic loading, the slope surface displacement and acoustic emission parameters exhibited a non-linear increase with the increase in the input wave amplitude. The surface displacement and acoustic emission characteristics during the failure process of the steep bedding slope can be

divided into two stages: the slow increase stage and the sharp increase stage. When the input wave amplitude value was less than 0.4 g, the slope surface displacement and acoustic emission parameters slowly increased; when the input amplitude reached 0.4 g, the slope surface displacement and the acoustic emission parameters significantly increased.

4. Under seismic wave action, a miniscule tension crack first appeared in the rock layer at the shoulder of the slope. When the seismic wave amplitude increased, the tension fracture extended downward along the rock layer and formed a locked segment at the toe of the slope. With the further increase in the seismic wave amplitude, the rock mass of the locked segment suddenly failed under the combined action of the seismic force and upper sliding body force. The shear section of the locked segment at the lower part of the landslide and the tensile cracks on the rock surface of the slope formed a through sliding surface, and slope sliding failure occurred along the through sliding surface to the free-face direction. Moreover, under seismic wave action, the rock layer inside the top of the slope fractured layer by layer owing to the loss of restraint, which resulted in the slope undergoing further sliding failure.
5. The deformation evolution process of the steep bedding rock slope under seismic dynamic action can be divided into four stages: tensile cracks appear at the top of the slope; the tensile cracks extend downward along the layer to form a locked segment at the toe of the slope; the locked segment shear fractures through the sliding surface; the slope suddenly becomes unstable and slides. The failure mode of the steep bedding rock slope under seismic dynamic action is tension-shear sliding failure.

Acknowledgements This research work is sponsored by the National Key Research and Development Project of China (Grant No. 2019YFC1509704), the National Natural Science Foundation of China (Grant Nos. U1704243, 41741019, 41977249 and 42090052), Henan Province Science and technology research project (Grant No. 192102310006), Central Plains Science and Technology Innovation Leader Project (Grant No. 214200510030).

References

- Buckingham E (1914) On physically similar system: illustrations of the use of dimensional equations. *Phys Rev J Arch* 4(4):345–376
- Che AL, Yang HK, Wang B, Ge XR (2016) Wave propagations through jointed rock masses and their effects on the stability of slopes. *Eng Geol* 201:45–56
- Chen XQ, Cui P, Zhao WY (2011) Emergency response to the Tangjiashan landslide-dammed lake resulting from the 2008 Wenchuan Earthquake, China. *Landslides* 8:91–98

- Chen ZL, Hu X, Xu Q (2016) Experimental study of motion characteristics of rock slopes with weak intercalation under seismic excitation. *J Mt Sci* 13(3):546–556
- Chigira M, Wu XY, Inokuchi T, Wang GH (2010) Landslides induced by the 2008 Wenchuan earthquake, Sichuan, China. *Geomorphology* 118(3–4):225–238
- Cui SH, Pei XJ, Huang RQ (2018) Effects of geological and tectonic characteristics on the earthquake-triggered Daguangbao landslide, China. *Landslides* 15:649–667
- Dong JY, Yang GX, Wu FQ, Qi SW (2011) The large-scale shaking table test study of dynamic response and failure mode of bedding rock slope under earthquake. *Rock Soil Mech* 32(10):2977–2988 (in Chinese)
- Dong JY, Yang JH, Yang GX, Wu FQ, Liu HS (2012) Research on similar material proportioning test of model test based on orthogonal design. *J China Coal Soc* 37(1):44–49 (in Chinese)
- Dong JY, Yang JH, Wu FQ, Yang GX, Huang ZQ (2013) Large-scale shaking table test research on acceleration response rules of bedding layered rock slope and its blocking mechanism of river. *Chin J Rock Mech Eng* 32(S2):3861–3867 (in Chinese)
- Dong JY, Wang C, Huang ZQ, Yang JH, Xue L (2021) Dynamic response characteristics and instability criteria of a slope with a middle locked segment. *Soil Dyn Earthq Eng* 150:106889
- Fan G, Zhang JJ, Wu JB, Yan KM (2016) Dynamic response and dynamic failure mode of a weak intercalated rock slope using a shaking table. *Rock Mech Rock Eng* 49(8):3243–3256
- Gischig VS, Eberhardt E, Moore JR, Hungr O (2015) On the seismic response of deep-seated rock slope instabilities—insights from numerical modeling. *Eng Geol* 193:1–18
- Hsieh YM, Lee KC, Jeng FS, Huang TH (2011) Can tilt tests provide correct insight regarding frictional behavior of sliding rock block under seismic excitation? *Eng Geol* 122:84–92
- Hu XW, Huang RQ, Shi YB, Lv XP, Zhu HY, Wang XR (2009) Analysis of blocking river mechanism of Tangjiashan landslide and dam-breaking mode of its barrier dam. *Chin J Rock Mech Eng* 28(1):181–189 (in Chinese)
- Hu XW, Luo G, Lv XP, Huang RQ, Shi YB (2011) Analysis on dam-breaking mode of Tangjiashan barrier dam in Beichuan county. *J Mt Sci* 8(2):354–362
- Huang RQ, Pei XJ, Fan XM, Zhang WF, Li SG, Li BL (2012) The characteristics and failure mechanism of the largest landslide triggered by the Wenchuan earthquake, May 12, 2008, China. *Landslides* 9(1):131–142
- Huang RQ, Zhao JJ, Ju NP, Li G, Lee ML, Li YR (2013) Analysis of an anti-dip landslide triggered by the 2008 Wenchuan earthquake in China. *Nat Hazards* 68(2):1021–1039
- Janusz W, David KK, Lee CY (2011) Toward the next generation of research on earthquake-induced landslides: current issues and future challenges. *Eng Geol* 122:1–8
- Kidyayeva V, Chernomorets S, Krylenko I, Wei FQ, Petrakov D, Su PC, Yang HJ, Xiong JN (2017) Modeling potential scenarios of the Tangjiashan Lake outburst and risk assessment in the downstream valley. *Front Earth Sci* 11:579–591
- Latha GM, Garaga A (2010) Seismic stability analysis of a Himalayan rock slope. *Rock Mech Rock Eng* 43(6):831–843
- Li LQ, Ju NP, Zhang S, Deng XX, Sheng DC (2019) Seismic wave propagation characteristic and its effects on the failure of steep jointed anti-dip rock slope. *Landslides* 16(1):105–123
- Liu F, Fu XD, Wang GQ, Duan J (2012) Physically based simulation of dam breach development for Tangjiashan Quake Dam, China. *Environ Earth Sci* 65:1081–1094
- Liu HX, Xu Q, Li YR, Fan XM (2014) Response of high-strength rock slope to seismic waves in a shaking table test. *Bull Seismol Soc Am* 103(6):3012–3025
- Luo XQ, Ge XR (2008) Theory and application of model test on landslide. China Water Power Press, Beijing in Chinese

- Meguid MA, Saada O, Nunes MA (2008) Physical modeling of tunnels in soft ground: a review. *Tunn Undergr Space Technol* 23(2):185–198
- Nakajima S, Watanabe K, Shinoda M et al (2016) Consideration on evaluation of seismic slope stability based on shaking table model test. In: *The 15th Asian regional conference on soil mechanics and geotechnical engineering*, Tokyo, vol 1. Japanese Geotechnical Society Special Publication, Tokyo, pp 957–962. <https://doi.org/10.3208/jgssp.JPN-100>
- Ning Y, Zhang G, Tang H, Shen W, Shen P (2019) Process analysis of toppling failure on anti-dip rock slopes under seismic load in southwest China. *Rock Mech Rock Eng* 52:4439–4455
- Panah AK, Eftekhari Z (2021) Shaking table tests on polymeric-strip reinforced-soil walls adjacent to a rock slope. *Geotext Geomembr* 49(3):737–756
- Qi SW, Lan HX, Dong JY (2015) An analytical solution to slip buckling slope failure triggered by earthquake. *Eng Geol* 194(S1):4–11
- Shi ZM, Guan SG, Peng M, Zhang LM, Zhu Y, Cai QP (2015) Cascading breaching of the Tangjiashan landslide dam and two smaller downstream landslide dams. *Eng Geol* 193:445–458
- Song DQ, Che AL, Zhu RJ, Ge XR (2018) Dynamic response characteristics of a rock slope with discontinuous joints under the combined action of earthquakes and rapid water drawdown. *Landslides* 15:1109–1125
- Srilatha N, Latha GM, Puttappa CG (2013) Effect of frequency on seismic response of reinforced soil slopes in shaking table tests. *Geotext Geomembr* 36:27–32
- Wang KL, Lin ML (2011) Initiation and displacement of landslide induced by earthquake—a study of shaking table model slope test. *Eng Geol* 122:106–114
- Wartman J, Riemer MF, Bray JD, Seed RB (1998) Newmark analyses of a shaking table slope stability experiment. In: *Proceedings of the geotechnical earthquake engineering and soil dynamics III*, ASCE. Geotechnical Special Publication No. 75, Seattle, pp 778–789
- Wartman J, Seed RB, Bray JD (2005) Shaking table modeling of seismically induced deformations in slopes. *J Geotech Geoenviron Eng* 131(5):610–622
- Whitman RV, Lambe PC (1986) Effect of boundary conditions upon centrifuge experiments using ground motions simulations. *Geotech Test J* 9:61–71
- Xu Q, Liu HX, Zou W, Fan XM, Chen JJ (2010) Study on slope dynamic response of accelerations by large-scale shaking table test. *Chin J Rock Mech Eng* 29(12):2420–2428 (in Chinese)
- Xu WJ, Xu Q, Wang YJ (2013) The mechanism of high-speed motion and damming of the Tangjiashan landslide. *Eng Geol* 157:8–20
- Yang GX, Qi SW, Wu FQ, Zhan ZF (2017) Seismic amplification of the anti-dip rock slope and deformation characteristics: a large-scale shaking table test. *Soil Dyn Earthq Eng*. S0267726116305772
- Yang Z, Tian X, Jiang Y, Liu X, Hu Y, Lai Y (2020) Experimental study on dynamic characteristics and dynamic response of accumulation slopes under frequent microseisms. *Arab J Geosci* 13:770
- Zhao LH, Liu XN, Mao J, Shao LY, Li TC (2020) Three-dimensional distance potential discrete element method for the numerical simulation of landslides. *Landslides* 17:361–377

Publisher's Note Springer Nature remains neutral with regard to jurisdictional claims in published maps and institutional affiliations.